Chapter 3

Precision Sequence Control in Bioinspired Peptoid Polymers

Jing Sun, Caroline Proulx, and Ronald N. Zuckermann*

Molecular Foundry, Lawrence Berkeley National Laboratory, Berkeley, California 94720
***E-mail: rnzuckermann@lbl.gov**

'Recent advances in solid-phase organic synthesis are shrinking the gap between biopolymers and traditional polymers. It is now possible to synthesize synthetic polymers with exact control over main chain length and monomer sequence, which is leading to a new class of information-rich materials. Peptoids are a particularly promising bio-inspired polymer platform because of their highly efficient synthesis and ready availability of starting materials. Hundreds of chemically diverse side chains can be introduced from simple building blocks, allowing their properties to be finely tuned. The peptoid platform allows the systematic investigation of new materials that are intermediate between proteins and bulk polymers, in both their structure and their properties. Here we review recent examples of peptoid polymers where the polymer properties are the direct result of the specific monomer sequence.

Introduction

During the past few decades, advances in polymer synthesis have significantly increased the degree of control over their structure. Great efforts have been made on new generations of functional polymeric materials by design at the molecular level (*1–4*). However, in comparison to biological polymers, current polymerization techniques offer a lower level of structural control. Biomacromolecules, like DNA, RNA and proteins, are distinct in that they are sequence-defined – they have precise monomer sequences, and absolute monodispersity. As a result, they often have complex tertiary folded structures,

In Sequence-Controlled Polymers: Synthesis, Self-Assembly, and Properties; Lutz, et al.;
ACS Symposium Series; American Chemical Society: Washington, DC, 2014.

and are capable of incredibly sophisticated functions, like information storage, molecular recognition and catalysis.

Bio-inspired polymers are an emerging class of materials that borrow from the most fundamental of design rules from nature to produce chemically diverse heteropolymers of defined length and sequence. Polypeptoids are a promising class of peptidomimetic polymers based on an N-substituted glycine backbone (*5–16*). The polypeptoid has an identical backbone to a polypeptide, but the side chain is covalently attached to the amide nitrogen. It thus lacks both chirality and hydrogen-bonding capacity in the backbone (*17*, *18*), which reduces complexity and offers tremendous advantageous properties for material studies, e.g. flexibility of the main chain (*18*, *19*), processible thermal properties (*18*), and good solubility in common solvents. The properties of the polypeptoid are highly dependent on the choice of side chains that allows for simplicity and freedom of design. The polypeptoid material is also biocompatible and exhibits potent biological activities with enhanced stability to proteolysis in comparison to a polypeptide (*20–22*).

Based on the well-established Merrifield method of solid-phase peptide synthesis (SPPS), Zuckermann et al. developed a two-step submonomer synthetic method that precludes main chain protecting groups (Figure 1) (*5*, *6*, *23–25*). In the first step, acylation of a resin-bound amine is performed with a haloacetic acid, with bromoacetic acid being generally preferred (*26*). The second step is an S_N2-type displacement reaction with a primary amine, which introduces the side chain. As hundreds of primary amines are readily available, a tremendous range of chemical diversity of is accessible. Both steps can be undertaken under very mild conditions that allow for facile manual or automated synthesis, with most commercial peptide synthesizers being able to accomplish the synthesis of polypeptoids. Zuckermann et al. built and optimized custom robotic synthesizers for fully automated synthesis of polypeptoids (*5*, *27*). With such a synthesizer, peptoid compounds can either be made in parallel or combinatorial libraries of high complexity can be synthesized by the 'mix & split' method. Combinatorial synthesis allows a very large number of peptoid chains to be generated in a single run where each individual resin bead contains a single compound (*28–30*). They have also developed mass spectrometry-based sequencing methods to sequence the peptoid on each bead, which greatly facilitates the screening of peptoids for new functions (*31*, *32*).

In general, polypeptoids exhibit high coupling efficiency (> 99% per monomer addition cycle), enabling up to 50 monomers to be added sequentially in good yields (*11*, *33*). However, longer chains (> 50 monomers) are challenging. Instead, the chemical conjugation of short segments has been used for the synthesis of long chains of polypeptoids (*34*). For example, azide-alkyne click chemistry was used to obtain a chain length of 100 monomers by coupling two 50mers together (*35*). It is worth mentioning that classical bulk polymerization of N-carboxyanhydrides allows for large-scale synthesis of longer chain length peptoids on a larger scale, but with less control (*13*, *14*, *36*).

Polypeptoids can thus be thought of as an information-rich polymer, where the structural precision of biopolymers is combined with the chemical diversity and robustness of traditional synthetic polymers. The ability to synthesize precise sequences will greatly benefit the investigation on the relationship of

In Sequence-Controlled Polymers: Synthesis, Self-Assembly, and Properties; Lutz, et al.;
ACS Symposium Series; American Chemical Society: Washington, DC, 2014.

structure and properties in polymeric materials on different levels, and enable further explorations of new generations of highly functional materials. In this book chapter, we will summarize recent advances in using peptoids to address fundamental issues in both polymer science and biomimetic nanoscience.

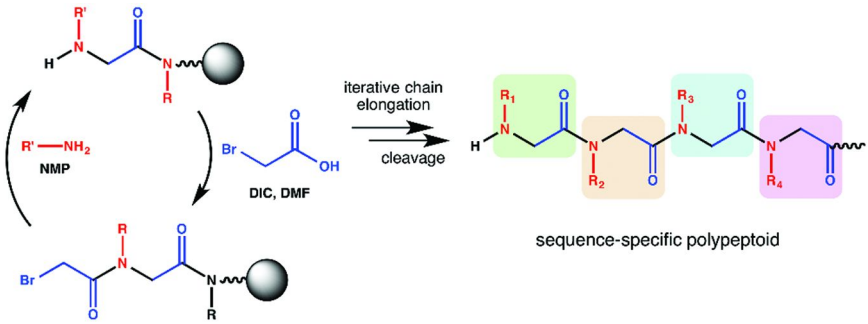

Figure 1. The solid-phase submonomer method allows the rapid synthesis of polypeptoids by a repeating two-step monomer addition cycle of acylation followed by nucleophilic S_N2 displacement with primary amines. Reproduced with permission from reference (16). Copyright (2013) American Chemical Society.

Sequence Control over Properties and Self-Assembly in Peptoid Polymers

In recent years, interest in polymer science has focused on new functional design at the molecular level (*37–40*), where precise architectural control during synthesis is key (*41–43*). Traditional polymerization techniques (e.g. radical and anionic polymerization) offer limited levels of control over chemical structures. Although many other techniques with a high-level of control have been explored (*10*, *41*, *44*, *45*), biologically inspired polymers, particularly polypeptoids, perhaps provide the most convenient platform. The sequence specificity and monodispersity of polypeptoids make them excellent candidates to elucidate the behavior of polymeric materials and the structure-property relationships.

Sequence Influence on Crystallization Behavior of Peptoid Polymers

Crystallization can strongly influence the physical properties of polymeric materials. Tunability of polymer crystallization is generally achieved through copolymerization, where comonomer content distribution in the polymer is key. Precisely controlled structure in peptoid polymers allows for different levels of control in crystallization behavior. Rosales et al. have studied the effects of comonomer compositions and distributions on crystallization behavior in series

In Sequence-Controlled Polymers: Synthesis, Self-Assembly, and Properties; Lutz, et al.;
ACS Symposium Series; American Chemical Society: Washington, DC, 2014.

of polypeptoids (*18*). The impact of side-chain size and comonomer distribution has been investigated. In general, it was found that increasing the side chain length induced melting temperature depression in these peptoid 15mers. For example, the addition of two carbons to the side chain depressed the melting transition by almost 15°C. Simultaneously, the crystallinity was readily controlled through the insertion of comonomers at precise locations along the polymer backbone. All of the above results are consistent with Flory's theory of crystallization (*46*). The sequence specificity leads to an increased understanding of the effects of comonomers on the crystallization behavior.

Sequence Influence on Microphase Separation of Peptoid Polymers

Microphase-separated block copolymers have a wide range of applications, such as templating, lithography and energy storage (*47*). In a diblock copolymer system A-B, the phase behavior may be controlled by three experimental parameters: the polymerization degree, the chemical composition, and the A-B Flory-Huggins parameter. All these parameters of the blocks can be readily controlled by the sequence of peptoid monomers.

One of the first microphase separation study focused on conjugates of polypeptoid with 2-methoxyethyl side chains ranging exactly from 18 to 48 monomers in length and polystyrene (*48*). These polystyrene-polypeptoid (SNme) block copolymers were shown to self-assemble into well-ordered hexagonally-packed cylinders and lamellae, as predicted by mean field theory for diblock copolymers. Furthermore, *N*-(2-phenylethyl)glycine (Npe) residues were incorporated to increase the miscibility with the polystyrene block. Despite the fact that the domain spacing of the S(Nme-Npe) diblock copolymer increased slightly, the strength of segregation decreased as the compatibility was increased.

Lately, Sun et al. designed a series of diblock co-polypeptoids with poly-*N*-2-(2-(2-methoxyethoxy)ethoxy)ethylglycine (pNte) as one of the blocks and poly-*N*-(2-ethyl)hexylglycine (pNeh) as the other block (*49*). With solid-phase synthesis, the chain length of all analogs was fixed at 36 monomers per chain, but the volume fraction of the pNte block was varied from 0.11 to 0.65 (Figure 2). This design allows the systematic investigation of the influence of side chains and monomer compositions. They are among the first groups to perform "fixed-length composition scans" on diblock copolymers that can quickly reveal interesting new phase behavior. Only lamellar and disordered morphologies were observed over the entire composition and temperature window examined. Moreover, the phase diagram of order-disorder transition temperature versus volume fraction of pNte (ϕ_{Nte}) exhibited a peak at $\phi_{Nte} = 0.24$, instead of 0.5 as expected from theory. This is possibly due to a composition-dependent parameter (χ) or the unique nature of the peptoid monomers. These results are in qualitative disagreement with all known theories of microphase separation in block copolymers that raises new questions about the intertwined roles of chemical structure of the monomerand polydispersity in the phase behavior of diblock copolymers.

In Sequence-Controlled Polymers: Synthesis, Self-Assembly, and Properties; Lutz, et al.;
ACS Symposium Series; American Chemical Society: Washington, DC, 2014.

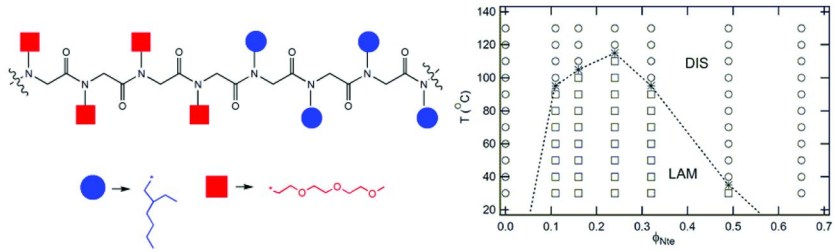

Figure 2. Structure of the diblock copolypeptoid and its phase diagram at different temperature and volume fractions, where DIS is disordered phase and LAM is lamellar phase. This unique phase diagram is different from all known theories of microphase separation in block copolymers.

Sun et al. also studied a series of crystalline diblock copolypeptoids poly-*N*-2-(2-(2-methoxyethoxy)ethoxy)ethylgly-cine (pNte)-*block*-poly-*N*-decylglycine (pNdc), where the pNdc block is crystalline (*50*). The block copolypeptoids self-assembles into a lamellar structure driven by the crystallization of the pNdc block (Figure 3). Interestingly, it is observed that the diblock copolymer can form two crystalline lamellae at room temperature, even though the pNte homopolymer is amorphous. More interestingly, the melting of both pNdc and pNte crystals is governed by the chain length of the pNdc block. This phenomenon could be due to the nearly identical molecular volumes of the side chains. The preorganization of the pNdc chains thus induces crystallization of the pNte chains. This study enhanced the understanding of block copolymer crystallization and proved that sequence-specific polypeptoid materials provide a unique platform to study the effect of composition and sequence design on physical properties and self-assembly of block copolymers.

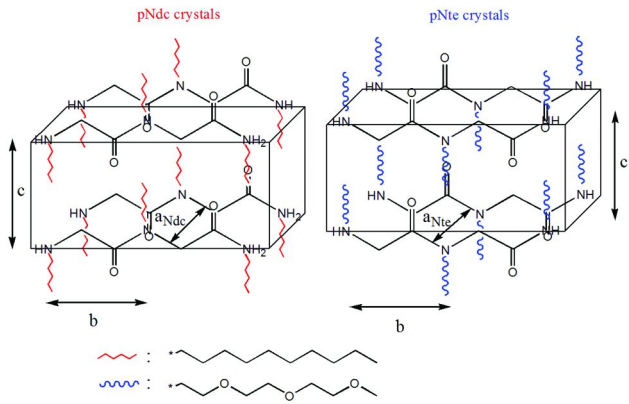

Figure 3. Two crystal structures of two blocks in diblock copolypeptoid. The formation of two crystalline lamellae at low temperatures is possible due to the nearly isosteric side chains of the two blocks. Reproduced with permission from reference (50). Copyright (2014) American Chemical Society.

In Sequence-Controlled Polymers: Synthesis, Self-Assembly, and Properties; Lutz, et al.;
ACS Symposium Series; American Chemical Society: Washington, DC, 2014.

Sequence Influence on Solution Self-Assembly of Peptoid Polymers

Solution self-assembly of block copolymers has been researched for years due to their potential applications in nanoscience and nanotechnology. The solid-phase synthetic approach enables highly tunable self-assembly behavior in block copolypeptoids (*51*).

Zuckermann and coworkers have developed model systems that allow controlled engineering of self-assembled structures in aqueous solution (*52*). They synthesized an amphiphilic diblock copolypeptoid system [*N*-(2-phenethyl)glycine]$_{15}$-*b*-[*N*-(2-carboxyethyl)glycine]$_{15}$ with one hydrophobic block of phenylethyl side chains and one chargeable hydrophilic block of carboxyethyl side chains. This diblock copolypeptoid first self-assembles into bilayer sheets and further twists into a superhelix structure at pH 6.5 (Fig. 4). The super helices remain remarkably robust homo-chiral structure in spite of the achiral nature of components.

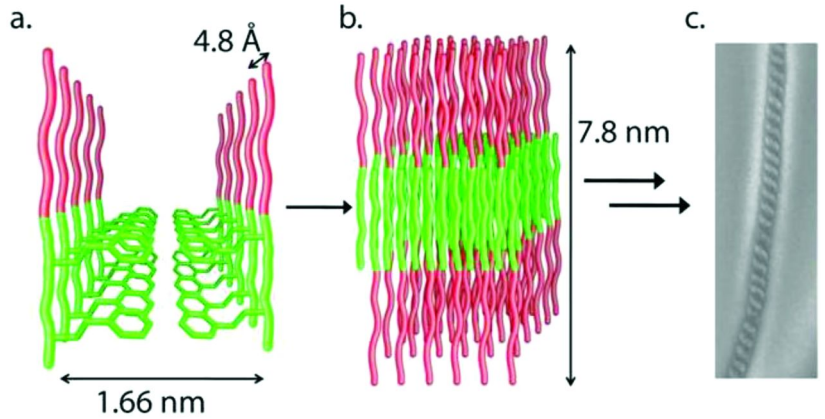

Figure 4. A model of the proposed superhelix self-assembly process. The chains initially crystallize with the aromatic groups facing each other (a). This spacing (1.66 nm) along with the distance between two chains laterally (4.8 Å) are verified in X-ray scattering. The chains further arrange into two-dimensional sheets (b) with a height of 7.8 nm as verified by AFM and X-ray scattering. The sheets are layered within the helices as evidenced by lamellar X-ray scattering of the fully formed superhelices. The green represents the hydrophobic portion of the chain while the red represents the hydrophilic block. Reproduced with permission from reference (52). Copyright (2010) American Chemical Society. (see color insert)

Solid-phase synthesis allows for facile synthesis of related analogs for investigation of the effect of ionic interactions and hydrogen bonding of the carboxyethyl side chains on the self-assembly of the superhelices. It is demonstrated that ionic interactions are critical for helix self-assembly to occur. Such systematic studies with exact structural control will benefit the study on self-assembly behavior of block copolymers in solution.

Sequence-Specific Polypeptoids for Applications in Material Science

Polypeptoid materials with precisely controlled structures and sequences are of particular interests for many applications ranging from biology to energy storage. Zoelen et al. studied tunable surface properties of polypeptoid-polystyrene block copolymers by systematically tuning the amount and sequence of fluorinated monomers for antifouling coating purposes (Figure 5) (*53*). They demonstrated that fluorinated polypeptoid chains dominated the free surface, where the presence of three fluorinated groups at the end of a 45mer peptoid chain allowed for maximal peptoid surface display. Surface reconstruction with three fluorinated groups is very fast. However, when the number of such group increases to five, it was found to be slower by an order of magnitude. They also reported a surface-exposed loop formation when fluorinated groups were located in the middle of the hydrophilic block. This study demonstrates that polypeptoid is a versatile platform for investigating surface properties of block copolymers for applications of antifouling-coating.

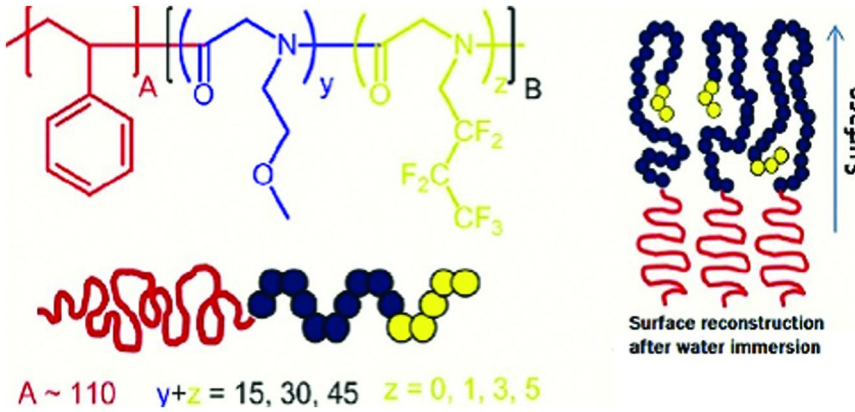

Figure 5. Schematic structures of block copolymers. Three fluorinated groups in peptoid sequences consisting of up to 45 hydrophilic monomers in length are needed to lower the surface energy of the peptoid and allow for its maximal surface segregation. Reproduced with permission from reference (53). Copyright (2012) American Chemical Society. (see color insert)

Poly(ethyleneoxide) (PEO)-based materials have received the most interest for solid polymer electrolyte application due to their high ionic conductivity. Efforts have been paid to optimize the thermal and electrical properties of such materials. Sun et al. designed a class of well-defined homopolypeptoids with controllable numbers of ethylene oxide units on the side chain (*54*). The polymer chain lengths were fixed at 20-monomers and the number of pendant (EO) units in the monomers ranged from one to three. This tunability of side chains enables the systematic study of the relationship between polymer structure and property. It was demonstrated that T_g values decreased with increasing side chain EO unit length. A very interesting crossover has been observed in the plot of T_g of

three polypeptoids versus *r* ratio (Li:EO). The ionic conductivity behavior of the complex of the polypeptoids and $Li[N(SO_2CF_3)_2$ salt has been subsequently explored. The highest ionic conductivity of 2.6 x 10^{-4} S/cm in this study was obtained in oligo-*N*-2-(2-(2-methoxyethoxy)ethoxy)ethylglycine–Li salt complex at 100°C, which is two orders of magnitude higher than PEO-mimetic polypeptides. Moreover, it is well demonstrated that the variations in conductivity of the system at a fixed temperature and salt concentration is dominated by T_g, and not other factors such as complexation with salts or chain length of (EO) units. It is proved that polypeptoid material with fine-tuned structure will, in a long run, offer great opportunity to explore new generation materials for many applications.

Mimicking proteins and peptides, amphiphilic peptoids have been used to control growth rate and morphology of calcite as a way to sequester CO_2. In a recent study, it was found that nanomolar concentrations of amphiphilic peptoids comprised of hydrophobic and anionic monomers were capable of enhancing calcite growth by up to 23-fold (*55*). The sequence, number of acidic side-chains, main chain length, and overall hydrophobicity, all influenced the ability of peptoids to affect calcite growth rate and morphology, with a variety of unique crystal shapes being observed (e.g. elongated spindles, twisted paddles, crosses, spheres). Interestingly, closely related analogs that each contained four substituted *N*-2-phenylethyl side chains at the N-terminus and eight *N*-2-carboxyethyl side-chains at the C-terminus, exhibited dramatically different influence on calcite growth depending on the nature of the phenyl ring substituents. This illustrates that subtle changes in the side-chain chemistry are enough to tune $CaCO_3$ mineralization growth rates and crystal morphology. Given the ease of synthesis and stability of peptoids, these analogs may find utility in templating $CaCO_3$ growth for application in atmospheric CO_2 sequestration.

Sequence Control in Biomimetic Materials

Two-Dimensional Peptoid Nanosheet Synthesis and Assembly

Sequence control in solid-phase peptoid synthesis enables the rational design of peptoid polymers that have the potential to self-assemble *via* non-covalent interactions, such as ionic and aromatic interactions. Given the lack of α carbon chirality and hydrogen bond donor at the nitrogen atom, the design element in peptoids has been exclusively focused on the nature of the side-chain functional groups. The widespread commercial availability of primary amines and the automated two-step submonomer protocol for peptoid synthesis has allowed the rapid construction of combinatorial peptoid libraries, leading to the discovery of materials exhibiting interesting properties. For example, in recent efforts, the Zuckermann laboratory explored the importance of sequence patterning of polar and nonpolar residues in the peptoid chain. Hydrophobic sequence patterning is known to be one of the primary determinants of protein structure (*56*), so libraries of peptoids were prepared in which the patterns were systematically varied. Interestingly, they identified a pair of amphiphilic peptoids that self-assembled into two-dimensional, 3 nm-thick nanosheet materials that are hundreds of micrometers in length and width (Figure 6) (*57*). These complimentary sequences

In Sequence-Controlled Polymers: Synthesis, Self-Assembly, and Properties; Lutz, et al.;
ACS Symposium Series; American Chemical Society: Washington, DC, 2014.

alternate between ionic and hydrophobic residues, such that the hydrophilic monomers are exposed to water, whereas the aromatic monomers form the bilayer's hydrophobic core. Assembly of the nanosheets occurs under dilute physiological conditions, and produces free-floating sheets that were characterized by numerous scattering and microscopy techniques.

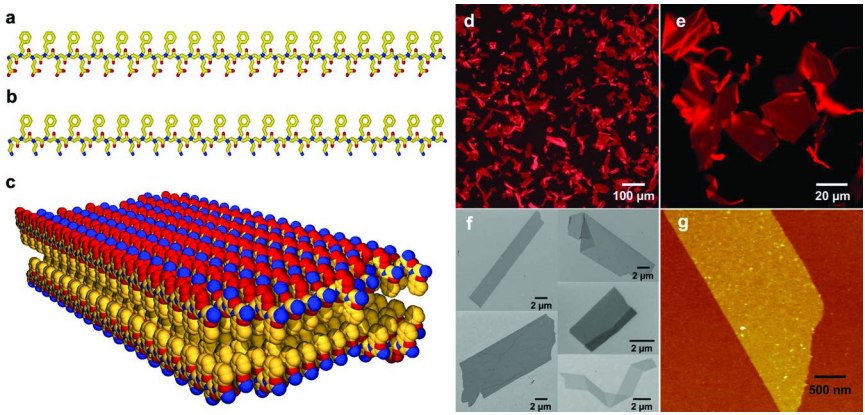

Figure 6. Two-dimensional crystalline sheets formed from two oppositely charged peptpoid polymers. Atomic color scheme: carbon, yellow; nitrogen, blue; oxygen, red. (a) Chemical structure of a negatively charged periodic amphiphilic peptoid, $(Nce\text{-}Npe)_{18}$. (b) Chemical structure of a positively charged periodic amphiphilic peptoid, $(Nae\text{-}Npe)_{18}$. (c) Molecular model of the sheets assembled from $(Nce\text{-}Npe)_{18}$ and $(Nae\text{-}Npe)_{18}$. The modelled conformation shows that hydrophobic groups face each other in the interior of the sheet and oppositely charged hydrophilic groups are alternating and surface-exposed. (d) Fluorescent optical microscope image of sheets stained with Nile Red (1μM) that are free-floating in aqueous solution. (e) Fluorescent optical microscope image of individual sheets. (f) SEM images of sheets on Si substrate. (g) Height-mode AFM image of a sheet. (see color insert)

The level of precision achieved by the automated, step-wise monomer addition cycles on solid-phase enables exact control over (1) the length of the designed peptoid chains, (2) the type of side-chain functionality, and (3) the exact monomer sequence. All of these were systematically varied to elucidate the factors that govern two-dimensional nanosheet assembly (Figure 7). For example, a length series of peptoid pairs 36, 18, 12 and 6 residues in length were synthesized, demonstrated that the sheet-forming capacity of peptoids below 12 residues in length decreased significantly, and that the optimal sheet-forming motif was 36 residues in length. Similarly, varying the sequence periodicity of the polar and nonpolar monomers while fixing the main chain length to 36 gave three sets of amphiphilic peptoid pairs: twofold [$(Nae\text{-}Npe)_{18}$ and $(Nce\text{-}Npe)_{18}$], threefold [$(Nae\text{-}Npe\text{-}Npe)_{12}$ and $(Nce\text{-}Npe\text{-}Npe)_{12}$], and fourfold [$(Nae\text{-}Npe\text{-}Npe\text{-}Npe)_{9}$ and $(Nce\text{-}Npe\text{-}Npe\text{-}Npe)_{9}$] sequences. Of the three above set of peptoid pairs, only the twofold sequence pair was able to assemble into

In Sequence-Controlled Polymers: Synthesis, Self-Assembly, and Properties; Lutz, et al.;
ACS Symposium Series; American Chemical Society: Washington, DC, 2014.

nanosheets. Moreover, in the twofold $(Nae\text{-}Npe)_{18}$ and $(Nce\text{-}Npe)_{18}$ sheet-forming system, the polar and apolar residues were systematically substituted by a neutral hydrophilic monomer, *N*-(2-methoxyethyl)glycine (Nme), in order to elucidate the importance of the charged and aromatic residues, respectively. These control experiments confirmed the crucial role of both the electrostatic interactions of the surface-exposed residues, as well as the aromaticity of the hydrophobic core. The nature of the hydrophobic monomer was varied further to give peptoid analogs with an all-benzyl hydrophobic residue composition, conserving the aromaticity but decreasing the overall side-chain length and conformational freedom. In this case, sheets assembly was unperturbed, and the sheet thickness decreased by 2 Å as expected by X-ray diffraction (XRD).

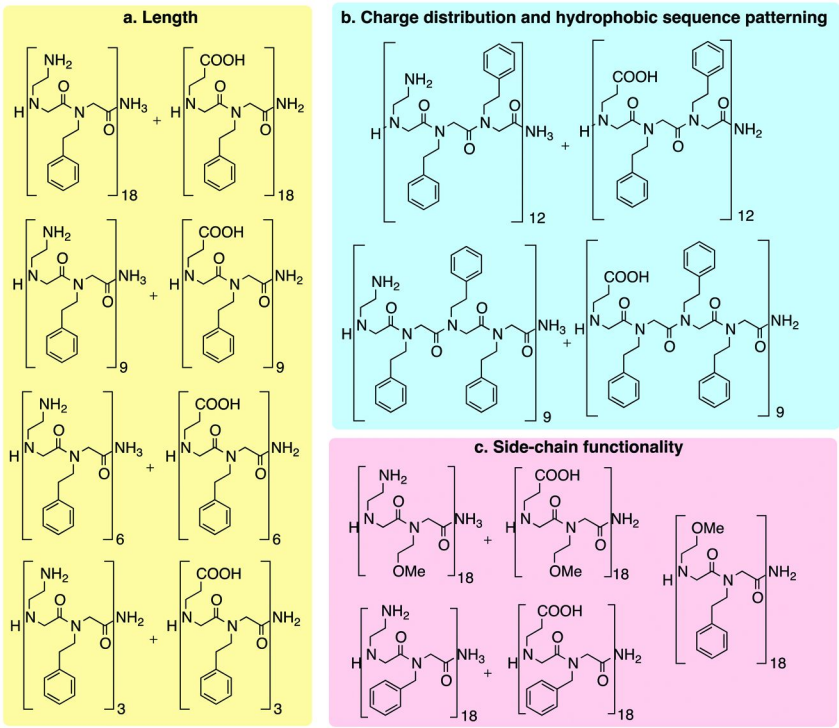

Figure 7. Peptoid sequences synthesized to study the effect of (a) length, (b) charge distribution, and (c) side-chain functionality on sheet-forming ability.

It was subsequently discovered that the nanosheet forming sequences could be simplified such that a single information-rich chain could be used to form nanosheets (*58*). A single-chain structure has a number of advantages, by avoiding the need to mix two strands, and easing the interpretation of analytical data and simplifying molecular modeling efforts. This was accomplished by combining the anionic and cationic residues into the same strand, by either (a) alternating the anionic and cationic residues in turn with the phenylethyl side-chain to give

(Nae-Npe-Nce-Npe)$_9$, or (b) by synthesizing a "block charge" peptoid, where the first half of the peptoid is positively charged and the second half is negatively charged (Nae-Npe)$_9$-(Nce-Npe)$_9$ (Figure 8).

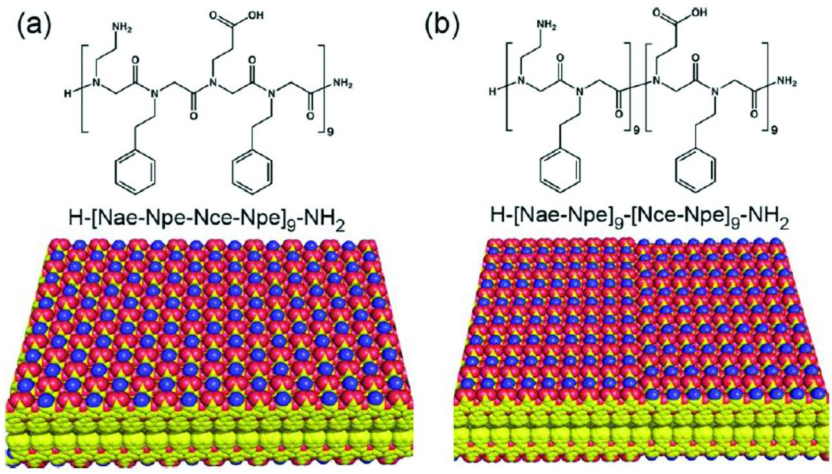

Figure 8. Single-chain peptoids that form nanosheets: (a) alternating charge and (b) block charge sequences. A model of a section of each type of sheet is shown, illustrating the differences in the proposed alignment of the chains. Although both designs can accommodate oppositely charged groups to be in close proximity, the alternating charge sheets would be expected to have less long-range order. Reproduced with permission from reference (58). Copyright (2011) Wiley. (see color insert)

Although it was found that both sequences were capable of assembling into nanosheets, differential pH and acetonitrile stability were detected in the two systems. Specifically, the nanosheets obtained from the alternating charge peptoid were less resistant to extreme pH variation and high percentage of organic solvent. The higher stability of the block charge nanosheets was rationalized by computer simulations, which showed more favorable electrostatic interactions could be achieved with this design.

Using Langmuir-trough isotherms and surface pressure measurements, a unique mechanism by which these nanosheet materials are produced was discovered (*59*). Notably, the amphiphilic peptoids were found to undergo: (1) adsorption at the air-water interface of a peptoid solution, followed by (2) compression into an ordered monolayer and (3) irreversible collapse of the monolayer to form stable, free-floating nanosheet bilayers. This process, which can occur by mechanical compression in a Langmuir-trough isotherm or by simply rotating vials from the horizontal to the vertical position using a custom-made "sheet rocker", can be repeated until over 95% of the peptoid is converted into nanosheets.

Peptoid Nanosheets as Antibody Mimetics

Given the robustness of the peptoid nanosheets, as well as the above-mentioned unique mode of assembly, it became apparent that they were ideal scaffolds for peptoid and peptide loops to be displayed on the nanosheet surface at precise intervals (*60*). As such, these materials could be designed to mimic antibodies and/or enzymes and engage in the multivalent binding of target molecules. It was envisioned that insertion of a hydrophilic sequence within a sheet-forming strand would lead to its exclusion from the bilayer scaffold during compression (Figure 9), and that positioning the loop insert in the middle would be less likely to disrupt sheet formation. In addition, a loop insert must not be too long or too hydrophobic in nature as to not hinder the adsorption at the air-water interface. Thus, precise sequence control over the position, nature, and length of the insert was an important element in designing artificial antibody mimetics.

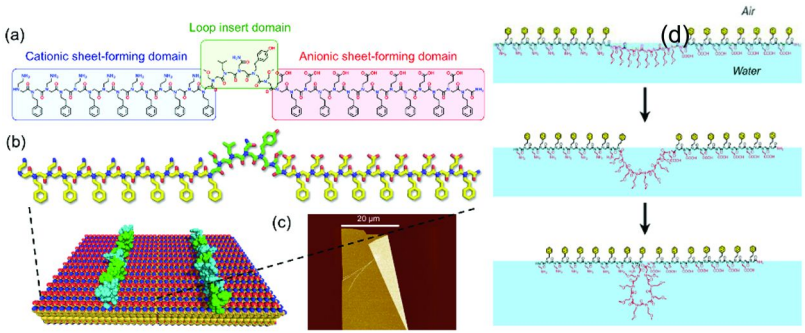

Figure 9. Peptoid nanosheets displaying a high density of conformationally constrained loops can be readily prepared by (a) flanking a random loop domain with sheet forming domains. (b) The amphiphilic pattern in the sheet-forming domains forms an extremely stable aromatic core that pushes the loop region onto the sheet surface. (c) The sheets are very uniform in structure as observed by AFM. (d) Mechanism of folding a linear peptoid sequence into a loop domain through compression of the peptoid monolayer at the air-water interface. (see color insert)

As a proof of concept, a series of 4, 8, and 12 consecutive neutral hydrophilic residues (*N*-(2-methoxyethyl)glycines, Nme) were inserted in the middle of the sheet-forming strand and tested for assembly. Expectedly, all of the above sequences formed nanosheets with predictable increases in sheet thickness and roughness detected by AFM. Using this strategy, peptidic loop-containing nanosheets could also be obtained, where the nature of the loop insert was tailored to bind protein and inorganic materials. In cases where the original

In Sequence-Controlled Polymers: Synthesis, Self-Assembly, and Properties; Lutz, et al.;
ACS Symposium Series; American Chemical Society: Washington, DC, 2014.

loop-containing peptoid designed was unable to form sheets, it was possible to tune the hydrophobicity of the peptoid chain by alternating biphenylethyl with phenylethyl side-chians in order to better compensate for the hydrophilic insert. The presence of peptide loops on the surface of the bilayer was confirmed by incubating the nanosheets with a mixture of proteases to selectively degrade the loop insertion, followed by AFM height measurements to corroborate a decrease in sheet thickness. Notably, the peptoid nanosheet scaffold remained intact under these harsh conditions. In addition, phosphorylation of a peptide loop substrate followed by incubation with FITC-labeled anti-phosphoserine antibody allowed fluorescent imaging of the nanosheets, thereby providing additional evidence of loop display. These materials hold great promise as molecular recognition elements for chemical and biological detection, and as templates for the growth of 2D materials. This work also highlights the importance of sequence control to predictably form a three-dimensional, antibody-like architecture from a carefully designed information-rich, linear peptoid.

Hydrophobic Sequence Patterning in Coil-to-Globule Transition

The use of peptoid polymers to study the folding process of globular proteins was recently reported, where the lack of hydrogen bond partners and chirality at the α carbon allowed for deconvolution of the hydrophobic effect from other competing factors in protein collapse (*35*). In accordance with the hydrophobic-polar (HP) protein folding model (*61*), where only two types of monomers, hydrophobic (H) and polar (P) are used, peptoid side-chains in this study were limited to either an *N*-methyl (blue, non polar) or *N*-2-carboxyethyl (red, polar) substituent (Figure 10a). Aside from the limited set of monomers used, several factors have been predicted to play important roles in globule formation, such as the H:P monomer ratio (*62*), the degree of hydrophobicity or hydrophilicity (*63*), the length of the polymer chain (*64*), the distribution of H and P monomers (*65*), as well as the ability for ionic interactions to occur. Solid phase synthesis allows precise control over all of the above parameters, with the intrinsic ability to design, synthesize, and ultimately compare peptoids with either blocky (protein-like) monomer distribution or repeating sequences (Figure 10b). Two monodisperse 50mers were ligated together to obtain a 100mer using a copper-catalyzed alkyne-azide cycloaddition reaction. The coil-to-globule transition of the two 100mers was then compared using a variety of techniques, including small angle X-ray scattering and acetonitrile titration, as well as dynamic light scattering measurements and fluorescence from environmentally sensitive dyes. These experiments revealed the formation of a tighter, more stable globule in the case of the protein-like sequence. Indeed, although both sequences appeared to form globules in aqueous solution, the protein-like sequence exhibited greater folding cooperativity by equilibrium acetonitrile titration and formed a more compact globule as determined by small-angle X-ray scattering.

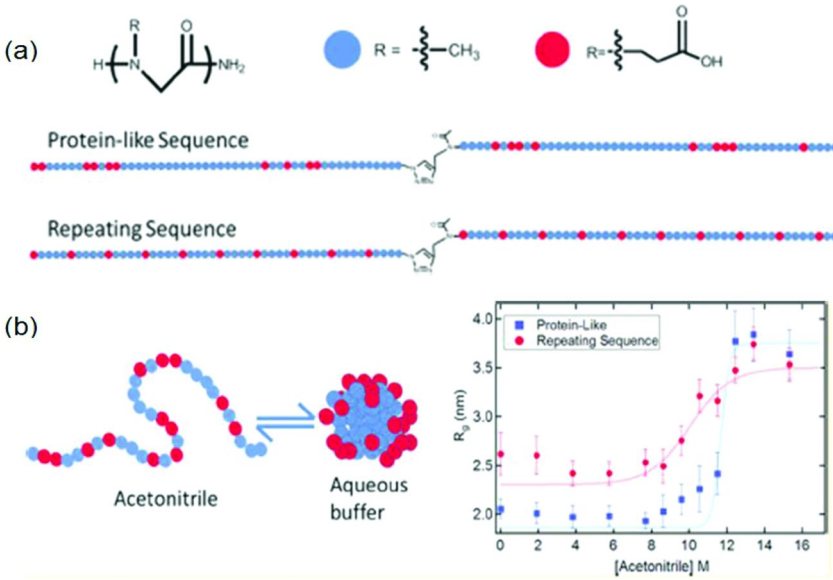

Figure 10. (a) Protein-like and repeating sequence polypeptoid 100mers. The polypeptoids were synthesized by clicking two HPLC-purified 50mers together. Each monomer is represented by a circle where the red circles are the hydrophilic and polar N-(2-carboxyethyl)glycine (P) monomer while the blue circles are non polar N-methylglycine (H) monomers. The protein-like sequence contains block sections of each type of monomer, while the repeating sequence has an even distribution of monomers. Both molecules have an identical composition of exactly 80 hydrophobic monomers and 20 hydrophilic monomers and a molecular weight of 8517 g/mol. (b) Protein-like sequence exhibited greater folding cooperativity by equilibrium acetonitrile titration and formed a more compact globule as determined by small-angle X-ray scattering. (see color insert)

Peptoid Helical Bundles

The degree of precision by which peptoid can be made has also permitted the design and synthesis of amphiphilic sequences adopting helical conformation (*51*). In this design, bulky, hydrophobic side-chains are patterned in a three-fold periodicity alternating with chiral hydrophilic monomers, and the main chain length is fixed at 15 residues to mimic the length of α helices observed in helical bundle proteins (Figure 11) (*66*). Varying the side-chain chemistry while keeping the hydrophobic patterning and main-chain length fixed, a one-bead-one compound combinatorial library was constructed using the "mix-and-split" method and a robotic synthesizer (*67*).

About 2.5% of the library in this study exhibited significant 1,8-ANS binding, which was used to assess the presence of a hydrophobic core. The MS/MS sequencing of 8 compounds revealed the importance of hydrophobic side chains with chiral α-methyl substitutions, but also found the diphenylethyl side chain to be prevalent.

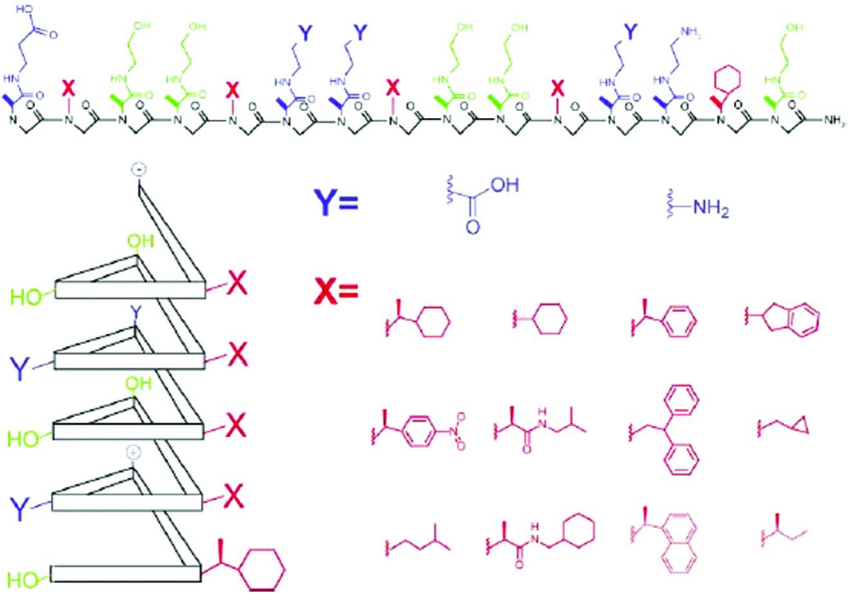

Figure 11. The 15-mer amphiphilic peptoid sequence with a 3-fold periodicity used as the combinatorial library scaffold, to screen for the assembly of helical bundles. Reproduced with permission from reference (51). Copyright (2002) Elsevier. (see color insert)

In a related study, one of the above 15mers, H-Nsace-Ndpe-Nsahe-Nsahe-Ndpe-Nsace-Nsaae-Nsch-Nsahe-Nsahe-Nspe-Nsace-Nsaae-Nsch-Nsahe-NH_2, was linked covalently together to form dimers, trimers, and tetramers *via* disulfide and oxime ligations (*34*). This approach was used to form single-chain helix bundles, where the incorporation of FRET pairs at each end facilitated the diagnosis of folded structures. It is oberved that several peptoids underwent cooperative transitions without disrupting helical secondary structure when tritrated with acetonitrile, suggesting the transitions to be a result of tertiary interactions forming a stable hydrophobic core similar to folded proteins. High affinity binding sites for zinc were later engineered into a linear peptoid sequence to obtain a functional helical bundle (*68*). Specifically, thiol and imidazole side-chains were incorporated such that zinc binding would only occur if a two-helix bundle was formed. The locations and numbers of thiols and imidazoles, as well as the monomer sequences and sizes of the loops connecting the two 15mers, were varied to enable sequence-structure-funciton relationships of zinc binding and selectivity. Some of the two-helix bundles studied were found to bind zinc with nanomolar affinity and high selectivity as compared to other divalent metal ions, such as Mg^{2+}, Mn^{2+}, Ca^{2+}, Ni^{2+}, Co^{2+}, Cu^{2+}, and Cd^{2+}.

Conclusion and Outlook

Polypeptoids are a unique, chemically diverse class of material closely related to polypeptides, in which the side-chain attachment point is shifted from the α carbon to the backbone nitrogen atom. This substitution has two major consequences: it removes chirality and a hydrogen bond donor (NH) from the backbone. Furthermore, this modification confers peptoids with an increased stability to both chemical and protease degradation. Although traditional synthetic polymers are equally robust and can be synthesized in bulk, their synthesis conditions preclude the formation of specific sequences or monodisperse polymers. Much like solid-phase peptide synthesis (SPPS), the step-wise submonomer approach for solid-phase peptoid synthesis allows polypeptoids to be synthesized with an exact length and sequence. This allows structure-properties studies to be conducted and clear design rules to be established to enforce specific behaviors and properties in peptoids (e.g. crystallization, microphase separation, self-assembly). In addition, there are hundreds of primary amines building blocks that are commercially available, enabling vast sequence diversity for the rapid discovery and tuning of novel materials.

In conjuction with experiment, tools for the predictive behavior of polypeptoids are currently being developed and have progressed tremendously in the past few years. Ramachandran plots of peptoids have been calculated and used to provide a preliminary picture of the peptoid folding landscape (*69*). The structures of several linear and cyclic peptoids have been successfully predicted using molecular dynamics simulations (*70*). Most recently, a custom forcefield derived specifically for peptoids (called MFTOID) has been developed a for CHARMM22 that enables accurate atomistic peptoid sumulations to be performed (*71*). The availability of these computational tools should begin to close the gap between experiment and prediction by dramatically enhancing the accuracy by which peptoid conformation can now be simulated. Structure prediction, in combination with the facile synthesis of peptoid polymers, sets the stage to further explore the impact of sequence-control in synthetic polymers for a wide range of applications.

Acknowledgments

This work was performed at the Molecular Foundry supported by the Office of Science, Office of Basic Energy Sciences, of the U.S. Department of Energy under Contract No. DE-AC02-05CH11231, and was also supported by the Defense Threat Reduction Agency under Contract No. IACRO-B1144571 .

References

1. Willner, I.; Zayats, M. *Angew. Chem., Int. Ed.* **2007**, *46*, 6408–6418.
2. Gomes, S.; Leonor, I. B.; Mano, J. F.; Reis, R. L.; Kaplan, D. L. *Prog. Polym. Sci.* **2012**, *37*, 1–17.
3. Shin, H.; Jo, S.; Mikos, A. G. *Biomaterials* **2003**, *24*, 4353–4364.

4. Esser-Kahn, A. P.; Iavarone, A. T.; Francis, M. B. *J. Am. Chem. Soc.* **2008**, *130*, 15820–15822.
5. Zuckermann, R. N. *Pept. Sci.* **2011**, *96*, 545–555.
6. Simon, R. J.; Kania, R. S.; Zuckermann, R. N.; Huebner, V. D.; Jewell, D. A.; Banville, S.; Ng, S.; Wang, L.; Rosenberg, S.; Marlowe, C. K. *Proc. Natl. Acad. Sci. U.S.A.* **1992**, *89*, 9367–9371.
7. Zuckermann, R. N. *Curr. Opin. Struct. Biol.* **1993**, *3*, 580–584.
8. Zuckermann, R. N.; Kodadek, T. *Curr. Opin. Mol. Ther.* **2009**, *11*, 299–307.
9. Kirshenbaum, K.; Zuckermann, R. N.; Dill, K. A. *Curr. Opin. Struct. Biol.* **1999**, *9*, 530–535.
10. Barron, A. E.; Zuckerman, R. N. *Curr. Opin. Chem. Biol.* **1999**, *3*, 681–687.
11. Murphy, J. E.; Uno, T.; Hamer, J. D.; Cohen, F. E.; Dwarki, V.; Zuckermann, R. N. *Proc. Natl. Acad. Sci. U.S.A.* **1998**, *95*, 1517–1522.
12. Lee, B. C.; Connolly, M. D.; Zuckermann, R. N. *Proc. NSTI Nanotech.* **2007**, *2*, 28–31.
13. Zhang, D.; Lahasky, S. H.; Guo, L.; Lee, C. U.; Lavan, M. *Macromolecules* **2012**, *45*, 5833–5841.
14. Luxenhofer, R.; Fetsch, C.; Grossmann, A. *J. Polym. Sci., Part A: Polym. Chem.* **2013**, *51*, 2731–2752.
15. Rosales, A. M.; Segalman, R. A.; Zuckermann, R. N. *Soft Matter* **2013**, *9*, 8400–8414.
16. Sun, J.; Zuckermann, R. N. *ACS Nano* **2013**, *7*, 4715–4732.
17. Rosales, A. M.; Murnen, H. K.; Kline, S. R.; Zuckermann, R. N.; Segalman, R. A. *Soft Matter* **2012**, *8*, 3673–3680.
18. Rosales, A. M.; Murnen, H. K.; Zuckermann, R. N.; Segalman, R. A. *Macromolecules* **2010**, *43*, 5627–5636.
19. Bradley, E. K.; Kerr, J. M.; Richter, L. S.; Figliozzi, G. M.; Goff, D. A.; Zuckermann, R. N.; Spellmeyer, D. C.; Blaney, J. M. *Mol. Divers.* **1997**, *3*, 1–15.
20. Lee, J.; Udugamasooriya, D. G.; Lim, H. S.; Kodadek, T. *Nat. Chem. Biol.* **2010**, *6*, 258–260.
21. Seo, J.; Lee, B. C.; Zuckermann, R. N. In *Comprehensive Biomaterials*; Ducheyne, P., Healy, K. E., Hutmacher, D. W., Grainger, D. W., Kirkpatrick, C. J., Eds.; Elsevier: 2011; Vol. 2, pp 53−76.
22. Fowler, S. A.; Blackwell, H. E. *Org. Biomol. Chem.* **2009**, *7*, 1508–1524.
23. Zuckermann, R. N.; Kerr, J. M.; Kent, S. B. H.; Moos, W. H. *J. Am. Chem. Soc.* **1992**, *114*, 10646–10647.
24. Zuckermann, R. N.; Figliozzi, G. M.; Banville, S. C.; Kerr, J. M.; Siani, M. A.; Martin, E. J.; Brown, E. G.; Wang, L. *Innovations and Perspectives in Solid-Phase Synthesis*; Epton, R., Ed.; Mayflower Worldwide Ltd.: Oxford, 1994; pp 397−402.
25. Uno, T.; Beausoleil, E.; Goldsmith, R. A.; Levine, B. H.; Zuckermann, R. N. *Tetrahedron Lett.* **1999**, *40*, 1475–1478.
26. Burkoth, T. S.; Fafarman, A. T.; Charych, D. H.; Connolly, M. D.; Zuckermann, R. N. *J. Am. Chem. Soc.* **2003**, *125*, 8841–8845.
27. Richter, L. S.; Spellmeyer, D. C.; Martin, E. J.; Figliozzi, G. M.; Zuckermann, R. N. *Comb. Pept. Nonpept. Libr.* **1996**, 387–404.

28. Zuckermann, R. N.; Martin, E. J.; Spellmeyer, D. C.; Stauber, G. B.; Shoemaker, K. R.; Kerr, J. M.; Figliozzi, G. M.; Goff, D. A.; Siani, M. A. *J. Med. Chem.* **1994**, *37*, 2678–2685.
29. Lam, K. S.; Lebl, M.; Krchnak, V. *Chem. Rev.* **1997**, *97*, 411–448.
30. Yu, P.; Liu, B.; Kodadek, T. *Nat. Biotechnol.* **2005**, *23*, 746–751.
31. Paulick, M. G.; Hart, K. M.; Brinner, K. M.; Tjandra, M.; Charych, D. H.; Zuckermann, R. N. *J. Comb. Chem.* **2006**, *8*, 417–426.
32. Thakkar, A.; Cohen, A. S.; Connolly, M. D.; Zuckermann, R. N.; Pei, D. *J. Comb. Chem.* **2009**, *11*, 294–302.
33. Lee, B. C.; Dill, K. A.; Zuckermann, R. N. *Polym. Prepr.* **2005**, *46*, 174–175.
34. Lee, B. C.; Zuckermann, R. N.; Dill, K. A. *J. Am. Chem. Soc.* **2005**, *127*, 10999–11009.
35. Murnen, H. K.; Khokhlov, A. R.; Khalatur, P. G.; Segalman, R. A.; Zuckermann, R. N. *Macromolecules* **2012**, *45*, 5229–5236.
36. Robinson, J. W.; Secker, C.; Weidner, S.; Schlaad, H. *Macromolecules* **2013**, *46*, 580–587.
37. Bellomo, E. G.; Wyrsta, M. D.; Pakstis, L.; Pochan, D. J.; Deming, T. J. *Nat. Mater.* **2004**, *3*, 244–248.
38. Pfeifer, S.; Zarafshani, Z.; Badi, N.; Lutz, J. F. *J. Am. Chem. Soc.* **2009**, *131*, 9195–9197.
39. Borner, H. G.; Schlaad, H. *Soft Matter* **2007**, *3*, 394–408.
40. Aida, T.; Meijer, E. W.; Stupp, S. I. *Science* **2012**, *335*, 813–817.
41. Lutz, J. F. *Nat. Chem.* **2011**, *2*, 84–85.
42. Sawamoto, M.; Kamigaito, M. *CHEMTECH (USA)* **1999**, *29*, 30–38.
43. Soeriyadi, A. H.; Boyer, C. A.; Nyström, F.; Zetterlund, P. B.; Whittaker, M. R. *J. Am. Chem. Soc.* **2011**, *133*, 11128–11131.
44. van Hest, J. C. M.; Tirrell, D. A. *Chem. Commun.* **2001**, 1897–1904.
45. Fetsch, C.; Luxenhofer, R. *Macromol. Rapid Commun.* **2012**, *33*, 1708–1713.
46. Flory, P. J. *Trans. Faraday Soc.* **1955**, *51*, 848–857.
47. Ruiz, R.; Kang, H.; Detcheverry, F. A.; Dobisz, E.; Kercher, D. S.; Albrecht, T. R.; de Pablo, J. J.; Nealey, P. F. *Science* **2008**, *321*, 936–939.
48. Rosales, A. M.; McCulloch, B. L.; Zuckermann, R. N.; Segalman, R. A. *Macromolecules* **2012**, *45*, 6027–6035.
49. Sun, J.; Teran, A. A.; Liao, X.; Balsara, N. P.; Zuckermann, R. N. *J. Am. Chem. Soc.* **2013**, *135*, 14119–14124.
50. Sun, J.; Teran, A. A.; Liao, X.; Balsara, N. P.; Zuckermann, R. N. *J. Am. Chem. Soc.* **2014**, *136*, 2070–2077.
51. Burkoth, T. S.; Beausoleil, E.; Kaur, S.; Tang, D.; Cohen, F. E.; Zuckermann, R. N. *Chem. Biol.* **2002**, *9*, 647–654.
52. Murnen, H. K.; Rosales, A. M.; Jaworski, J. N.; Segalman, R. A.; Zuckermann, R. N. *J. Am. Chem. Soc.* **2010**, *132*, 16112–16119.
53. van Zoelen, W.; Zuckermann, R. N.; Segalman, R. A. *Macromolecules* **2012**, *45*, 7072–7082.
54. Sun, J.; Stone, G. M.; Balsara, N. P.; Zuckermann, R. N. *Macromolecules* **2012**, *45*, 5151–5156.

55. Chen, C.-L.; Qi, J.; Zuckermann, R. N.; DeYoreo, J. J. *J. Am. Chem. Soc.* **2011**, *133*, 5214–5217.
56. Dill, K. A. *Biochemistry* **1990**, *29*, 7133–7155.
57. Nam, K. T.; Shelby, S. A.; Choi, P. H.; Marciel, A. B.; Chen, R.; Tan, L.; Chu, T. K.; Mesch, R. A.; Lee, B. C.; Connolly, M. D. *Nat. Mater.* **2010**, *9*, 454–460.
58. Kudirka, R.; Tran, H.; Sanii, B.; Nam, K. T.; Choi, P. H.; Venkateswaran, N.; Chen, R.; Whitelam, S.; Zuckermann, R. N. *Pept. Sci.* **2011**, *96*, 586–595.
59. Sanii, B.; Kudirka, R.; Cho, A.; Venkateswaran, N.; Olivier, G. K.; Olson, A. M.; Tran, H.; Harada, R. M.; Tan, L.; Zuckermann, R. N. *J. Am. Chem. Soc.* **2011**, *133*, 20808–20815.
60. Olivier, G. K.; Cho, A.; Sanii, B.; Connolly, M. D.; Tran, H.; Zuckermann, R. N. *ACS Nano* **2013**, *7*, 9276–9286.
61. Dill, K. A. *Biochemistry* **1985**, *24*, 1501–1509.
62. Ashbaugh, H. S. *J. Phys. Chem. B* **2009**, *113*, 14043–14046.
63. Siu, M.; Zhang, G.; Wu, C. *Macromolecules* **2002**, *35*, 2723–2727.
64. Jennings, D. E.; Kuznetsov, Y. A.; Timoshenko, E. G.; Dawson, K. A. *J. Chem. Phys.* **2000**, *112*, 7711–7722.
65. Dasmahapatra, A. K.; Nanavati, H.; Kumaraswamy, G. *J. Chem. Phys.* **2007**, *127*, 234901.
66. Presnell, S. R.; Cohen, F. E. *Proc. Natl. Acad. Sci. U.S.A.* **1989**, *86*, 6592–6596.
67. Zuckermann, R. N.; Kerr, J. M.; Siani, M. A.; Banville, S. C. *Int. J. Pept. Protein Res.* **1992**, *40*, 497–506.
68. Lee, B. C.; Chu, T. K.; Dill, K. A.; Zuckermann, R. N. *J. Am. Chem. Soc.* **2008**, *130*, 8847–8855.
69. Butterfoss, G. L.; Renfrew, P. D.; Kuhlman, B.; Kirshenbaum, K.; Bonneau, R. *J. Am. Chem. Soc.* **2009**, *131*, 16798–16807.
70. Butterfoss, G. L.; Yoo, B.; Jaworski, J. N.; Chorny, I.; Dill, K. A.; Zuckermann, R. N.; Bonneau, R.; Kirshenbaum, K.; Voelz, V. A. *Proc. Natl. Acad. Sci. U.S.A.* **2012**, *109*, 14320–14325.
71. Mirijanian, D. T.; Mannige, R. V.; Zuckermann, R. N.; Whitelam, S. *J. Comput. Chem.* **2014**, *35*, 360–370.